communications chemistry

Article

https://doi.org/10.1038/s42004-024-01371-4

Mechanistic investigation of sustainable heme-inspired biocatalytic synthesis of cyclopropanes for challenging substrates

Check for updates

Dongrun Ju, Vrinda Modi, Rahul L. Khade & Yong Zhang

Engineered heme proteins exhibit excellent sustainable catalytic carbene transfer reactivities toward olefins for value-added cyclopropanes. However, unactivated and electron-deficient olefins remain challenging in such reactions. To help design efficient heme-inspired biocatalysts for these difficult situations, a systematic quantum chemical mechanistic study was performed to investigate effects of olefin substituents, non-native amino acid axial ligands, and natural and non-natural macrocycles with the widely used ethyl diazoacetate. Results show that electron-deficient substrate ethyl acrylate has a much higher barrier than the electron-rich styrene. For styrene, the predicted barrier trend is consistent with experimentally used heme analogue cofactors, which can significantly reduce barriers. For ethyl acrylate, while the best non-native axial ligand only marginally improves the reactivity versus the native histidine model, a couple of computationally studied macrocycles can dramatically reduce barriers to the level comparable to styrene. These results will facilitate the development of better biocatalysts in this area.

Olefin cyclopropanation is a useful approach to synthesize cyclopropanes which are commonly used in the production and investigation of many pharmaceuticals and biologically active products[1–5]. The use of iron porphyrins, especially engineered heme proteins[6–48], can possess excellent catalytic cyclopropanation yields (up to 99%) and outstanding stereoselectivity (up to 99.9%). In addition, all engineered heme carbene transferases[6–14,16–18,21,22,37–47] work at room temperature, and they are naturally biocompatible. Together with the use of the most abundant and inexpensive transition metal (Fe) in these biocatalysts, these nice features support their applications in sustainable chemistry. However, the previously reported substrates are mostly electron-rich olefins, such as styrene (**1**) and its derivatives. The catalytic performance for electron-poor substrates is much worse[6,23,26,27,30,49–51]. For example, even with the assistance from the protein environment, the cyclopropanation yield (69%) of para-CF_3 substituted styrene with the widely used carbene precursor ethyl diazoacetate (EDA) using the best myoglobin-based catalyst is significantly inferior to the >99% yield for styrene itself. For unactivated olefins such as 1-octene (**2**), there is only one successful report to date for heme-based catalyst[17]. Even after screening ~50 heme proteins plus additional one to three rounds of mutagenesis, the catalytic reactivities for 1-octene are still quite low, since the total turnover numbers (TTNs) of 100–490[17] are significantly smaller than the TTN of ~47,000 for styrene[9]. As regards the typical electron-poor olefin such as ethyl acrylate (**3**, an important reagent to synthesize pharmaceutical molecules/intermediates), there is no report of successful catalytic cyclopropanation by using iron porphyrin or heme protein catalysts. Even using noble metal Ir-based porphyrins[52], the yields are still notoriously low, ~10–20%. Despite this, unactivated and electron-deficient olefins are attractive substrates for synthesis due to their low cost and limited reactivity, allowing for controlled selectivity[53]. Therefore, it is highly important and interesting to explore heme-inspired sustainable catalysts for such challenging substrates.

Recent computational work has provided useful information to understand heme-inspired cyclopropanations with iron porphyrin carbene (IPC) intermediates[14,19,20,32–34,38,40,47,54–59] as well as native heme enzymatic reactions[60–63] and non-heme protein reactions, including second-sphere effects[64,65]. For instance, the basic reaction pathway of the cyclopropanation of styrene for formally Fe^{II}-based hemes (or Fe^{III}-based hemes under reducing conditions) features a nonradical, concerted nonsynchronous mechanism[54]. Computational results also support the use of these heme catalysts as they were found to dramatically reduce the reaction barriers compared to the non-catalyzed ones by 20–30 kcal mol^{-1} (ref. 54). The second-sphere effects were found to be important in reproducing experimental heme carbene reaction stereoselectivity and chemoselectivity[33,34]. Nevertheless, to the best of our knowledge, no previous theoretical work has addressed the cyclopropanations of challenging substrates, such as 1-octene and especially ethyl

Department of Chemistry and Chemical Biology, Stevens Institute of Technology, 1 Castle Point Terrace, Hoboken, NJ, 07030, USA.
e-mail: yzhang37@stevens.edu

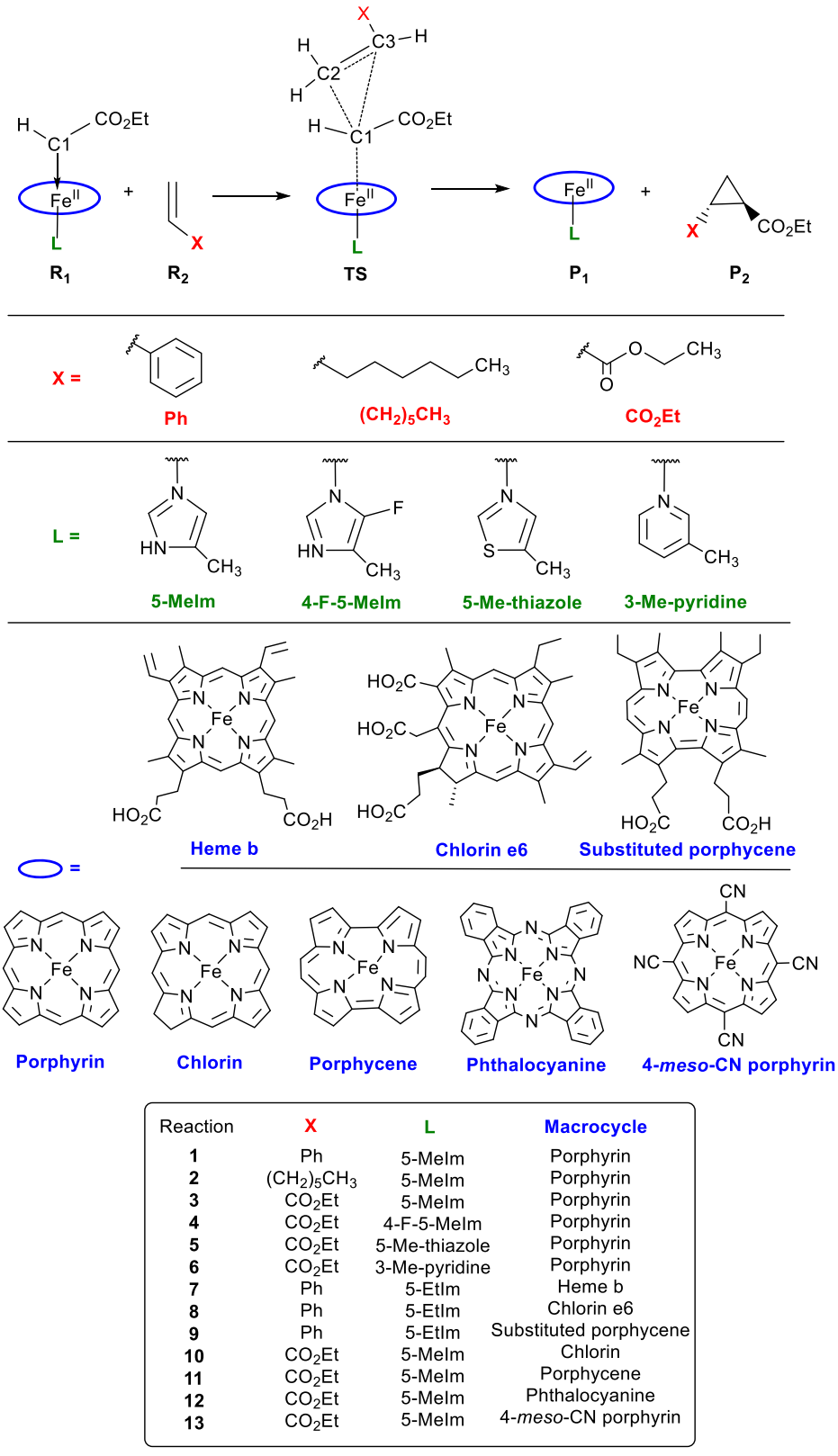

Fig. 1 | Fe^{II}-macrocycle catalyzed cyclopropanations of olefins in reactions 1–13. The reaction features a concerted mechanism, in which X represents the substrate substituent, L represents the axial ligand, and the blue oval represents the macrocycle.

Reaction	X	L	Macrocycle
1	Ph	5-MeIm	Porphyrin
2	$(CH_2)_5CH_3$	5-MeIm	Porphyrin
3	CO_2Et	5-MeIm	Porphyrin
4	CO_2Et	4-F-5-MeIm	Porphyrin
5	CO_2Et	5-Me-thiazole	Porphyrin
6	CO_2Et	3-Me-pyridine	Porphyrin
7	Ph	5-EtIm	Heme b
8	Ph	5-EtIm	Chlorin e6
9	Ph	5-EtIm	Substituted porphycene
10	CO_2Et	5-MeIm	Chlorin
11	CO_2Et	5-MeIm	Porphycene
12	CO_2Et	5-MeIm	Phthalocyanine
13	CO_2Et	5-MeIm	4-*meso*-CN porphyrin

acrylate, for which most previous experimental efforts have yet to achieve excellent catalytic performance.

Given this situation, a systematic computational mechanistic investigation was performed to 1) reveal specific reactivity differences among three characteristic substrates: the electron-rich styrene, the unactivated 1-octene, and the electron-deficient ethyl acrylate, in reactions **1**–**3**; 2) examine effects of structural components of the Fe^{II}-based hemes in the active sites of engineered biocatalysts on cyclopropanations, including both various axial ligands (reactions **3**–**6**) and equatorial ligands (reactions **7**–**13**), as shown in Fig. 1. With regard to axial ligands, previous experimental and computational work have shown that the presence of an axial ligand enhances the cyclopropanation reactivity, with the neutral His being more effective than the negative charged Cys ligand[54]. Thus, this work explores the use of several non-native, neutral, N-based axial ligands in

Table 1 | Key free energy, charge, and geometry parameters in the cyclopropanation pathways[a]

Reaction	ΔG (kcal mol^{-1})	$\Delta G^{\ddagger,b}$ (kcal mol^{-1})	ΔG° (kcal mol^{-1})	ΔR_{FeC1} (Å)	ΔR_{C2C3} (Å)	ΔQ_{C1} (e)	Q_{CT}[c] (e)
1[d]	9.24	13.41	−56.65	0.108	0.014	−0.146	0.179
2	9.68	14.08	−58.27	0.114	0.013	−0.144	0.191
3	13.11	17.56	−59.90	0.143	0.018	−0.186	0.159
4	12.79	17.53	−61.69	0.149	0.019	−0.192	0.168
5	13.50	18.04	−60.58	0.147	0.018	−0.193	0.169
6	14.19	18.59	−60.48	0.153	0.019	−0.193	0.176
7	8.41	13.14	−56.23	0.103	0.014	−0.144	0.178
8	5.75	10.58	−54.52	0.104	0.014	−0.138	0.162
9	5.31	10.28	−53.15	0.116	0.015	−0.139	0.182
10	9.46	15.09	−63.79	0.138	0.019	−0.188	0.162
11	14.53	18.73	−55.31	0.144	0.020	−0.195	0.169
12	12.33	15.96	−50.63	0.137	0.016	−0.176	0.189
13	9.26	13.56	−59.30	0.122	0.010	−0.169	0.174

[a]Changes are those at the transition state compared with reactants.
[b]Free energy barriers from high-level, single point calculations.
[c]Charge transfer (CT) magnitude from the olefin moiety to C1.
[d]All results of reaction 1 except for the high-level barrier are from ref. 54.

reactions **4–6** with comparison to the His model (5-methylimidazole, 5-MeIm, used previously[33,34,54]) in reaction **3**, including an electron-withdrawing substituent on 5-MeIm (**4**), a different heteroatom in the five-membered ring (**5**), and a six-membered ring (**6**). Recent experimental studies demonstrate the beneficial effect of various macrocycles, other than heme b, in catalyzing cyclopropanation[14,15,42,66]. Therefore, we first compared three experimentally studied cofactors in reactions **7–9**, followed by several different macrocycles on the cyclopropanation reaction with the most challenging substrate, ethyl acrylate, in reactions **10–13**.

To ensure the comparisons are made on the same footing and to focus on the effects of the aforementioned structural variations, all reactions use IPCs generated from the same carbene precursor, EDA, as used in many experimental studies. Moreover, the concerted mechanism found in the same and many similar heme carbene cyclopropanations from both experimental and computational studies[19,33,34,40,47,54] was used for all these reactions: proceeds from two reactants ($\mathbf{R_1}$: IPC; $\mathbf{R_2}$: substrate) through a transition state (**TS**) and to form the products ($\mathbf{P_1}$: recycled catalyst; $\mathbf{P_2}$: cyclopropane). The selected basis set and range-separated hybrid DFT functional with dispersion correction (See Methods for details) has enabled numerous accurate predictions of experimental properties of heme carbenes and their reactivities, stereoselectivities, regioselectivities, and chemoselectivities[33,34,47,54,67–71]. Results from this work not only reproduced existing experimental trends, but more importantly, revealed the effects of non-native axial ligands and macrocycles, which had not been previously reported, regarding their potential applications in addressing difficult electron-deficient substrates to facilitate the development of sustainable cyclopropanation biocatalysts for challenging substrates. It should be noted that the protein environment is important to determine the final biocatalytic reactivity, and our work here, as the first study for such challenging reactions, is focused on the effects of cofactor structures, not protein mutation-related reactivity/selectivity data.

Results and discussion

Since there are no experimental reaction barrier data in this area to provide benchmark results, in our previous computational method development, we investigated a number of DFT functionals and basis sets[67,69] by evaluating both the qualitative predictions of many reaction trends and quantitative predictions of many spectroscopic properties and non-barrier reaction quantities (such as kinetic isotope effect (KIEs), enantiomeric excess (ee), diastereomeric excess (de)). Our results show that the range-separated hybrid DFT ωB97XD functional with dispersion correction enabled excellent quantitative predictions of experimental X-ray geometries with 1.0% mean percentage deviation[69], demonstrated excellent correlation with experimental ^{13}C NMR shifts ($R^2 = 0.9691$)[67]. More importantly it reproduced the qualitative reactivity trends for experimental (1) IPC formation[69], (2) C-H insertion[68], (3) cyclopropanation[54], (4) Si-H insertion[70], (5) chemoselectivity of cyclopropanation vs. C-H insertion[34], (6) diastereoselectivity of cyclopropanation[54], and quantitative predictions of KIEs for C-H insertion[68], cyclopropanation[54], and Si-H insertion[70], and ee and de data of cyclopropanations with 1% error[33] for a wide range of substrates.

To further evaluate this method, we performed additional high-level calculations of free energy barriers (Table 1) using a large basis of 6-311 + + G(2 d,2p) for all atoms (see Method for details). Although these barriers are larger than those from using the current basis with the same DFT method by 4.54 kcal mol^{-1} on average, they have excellent correlations, as seen from Fig. 2 with a linear correlation coefficient $R = 0.99$. This comparative study shows that although the barriers can be affected by the used methods and absolute values from the current method may be lower, their trends are basically the same. These results support the efficient use of the current method as in previous studies of heme carbene reactions[33,34,47,54,67–71] in the subsequent work.

Substrate substituent effect

In this section, the cyclopropanation pathways for three different olefins, with porphyrin as the macrocycle and 5-MeIm as the axial ligand for His, as used in many prior studies[20,33,40,47,54,59,70], were investigated (reactions **1–3**). As shown in Fig. 2, cyclopropanation is less favorable with the unactivated olefin **2** (X = $(CH_2)_5CH_3$) and especially olefin **3** (X = CO_2Et). Their energy barriers, measured as Gibbs free energy of activation ($\Delta G^{\ddagger}$) (see Table 1), higher than that of olefin **1** (X=Ph), respectively. These barrier differences alone lead to ~2 and ~700 (~3 and ~1000 at the high-level) folds smaller rate constants or slower reactivities based on the Eyring equation at room temperature (scaling with exp(-$\Delta G^{\ddagger}$/RT)), indicating the challenging nature of especially electron-deficient olefins for cyclopropanations. The reaction energies (ΔG°s) in Table 1 indicate that they are all thermodynamically favorable.

The key geometric and charge changes for reactions **2** and **3** are in the inserts of Fig. 3 and Fig. 4a, respectively, and exhibit similar trends to the most significant changes observed in reaction **1**, reported previously[54]. The largest geometric change is the elongation of the iron-carbene distance (ΔR_{FeC1} = 0.108, 0.114, 0.143 Å, respectively for reactions **1–3**), which is to accommodate the attack of the carbene group on the C=C bond of olefins[54]. The ca. 10-fold smaller change of the C=C bond (ΔR_{C2C3} ~ 0.015 Å) in **TS** from reactant compared to that from product (~0.16 Å, see Supplementary

Table 4) indicates an early transition state as reported recently for similar heme carbene cyclopropanations[54]. Interestingly, the barrier trend has an excellent correlation with ΔR_{FeC1} (the linear correlation coefficient $R^2 = 0.9968$) and indicates that **TS(3)** (the reaction number is in parenthesis) has the least early transition state feature, corresponding to the highest barrier. It can be seen from Fig. 3 and Fig. 4a that the largest atomic charge change is for the carbene's carbon C1 (atom number shown in Fig. 1), and the most significant charge transfer (CT) from reactants to **TS** lies with the charge donation from olefin to C1, the same as found for other heme carbene cyclopropanations[54]. These features also show the electrophilic nature as observed experimentally in the same and similar heme catalytic reactions[9,23,26,27]. Therefore, it is understandable that the electron-deficient substrate **3** causes the highest difficulty for this type of electrophilic reaction. In fact, its electron-withdrawing CO_2Et moiety hinders the charge transfer from the olefin to C1, as evidenced by a much smaller CT of 0.159 *e* compared to 0.179 *e* and 0.191 *e* for reactions **1** and **2** (see Table 1). These results provide a detailed understanding of the electronic nature of this challenging reaction, which has not been reported experimentally yet.

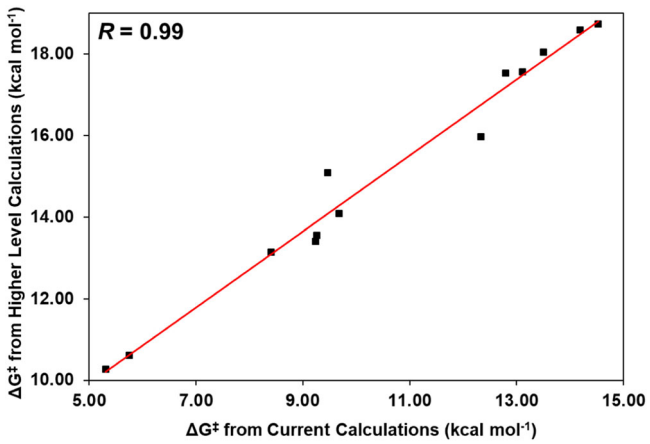

Fig. 2 | Correlation between current and higher-level free energy barriers of reactions 1–13. The trendline (in red) shows a strong correlation between the barriers obtained from the two different levels of calculations.

Axial ligand effect

Both computational and experimental work shows that axial ligands can be used to modulate cyclopropanation reactivity, with the best one being the native amino acid His when styrene is the substrate[46,54]. Here, we explore variations of the N-based neutral ligand (the best platform from prior experimental and computational work) compared to non-native ones in catalyzing the cyclopropanation of the most challenging substrate here, to determine if further improvements can be achieved.

Based on the electronic driving force in these electrophilic reactions, as illustrated by the dominant CT from olefin to carbene in Figs. 3–4, we hypothesize that an electron-withdrawing substituent on His (modeled here as 5-MeIm) will enhance its electrophilicity. As shown in Fig. 4, using 4-F-5-MeIm (we choose F due to its small size to maintain a stable binding of this ligand to Fe) indeed makes C1 more positively charged in IPC by ~0.01 *e* (see Supplementary Table 9), which causes an increase of $|Q_{CT}|$ by ~0.01 *e* as expected (see Table 1). This is associated with a corresponding barrier reduction of 0.32 kcal mol^{-1}, or ~2-fold increase in rate constant at room temperature according to Eyring's equation. We then investigated 5-Me-thiazole (5-methylthiazole) to examine the effect of the non-coordinating heteroatom in the axial ligand ring, which does not show improvement and rather a small increase in $\Delta G^{\ddagger}$ (see Fig. 4). Compared to these five-membered ring systems, the six-membered ring 3-Me-pyridine (3-methylpyridine) has the worst reactivity. It is interesting to note that the significantly lower reactivity of this pyridine-based ligand compared to the His mimic in cyclopropanations of ethyl acrylate, aligns with the experimentally observed much lower yield for this non-native ligand vs. His in cyclopropanations of styrene[46]. This suggests that the axial ligand effects on cyclopropanations of different substrates remain the same.

The geometric changes for **TS(3–6)** relative to reactants shown in Fig. 4 indicate the same early transition state features. The most significant change is still the elongation of iron-carbene distance (ΔR_{FeC1}), but the range is smaller than that for the substrate substituent effect, consistent with the smaller barrier range for the studied axial ligand effect here. The linear correlation coefficient R^2 for barriers vs. ΔR_{FeC1} for these six reactions (**1–6**) with the same porphyrin macrocycle is still high, 0.97. The charge diagrams in Fig. 4 also show consistent features: the same largest atomic charge change for C1 and the same greatest CT from olefin to carbene, but with smaller ranges.

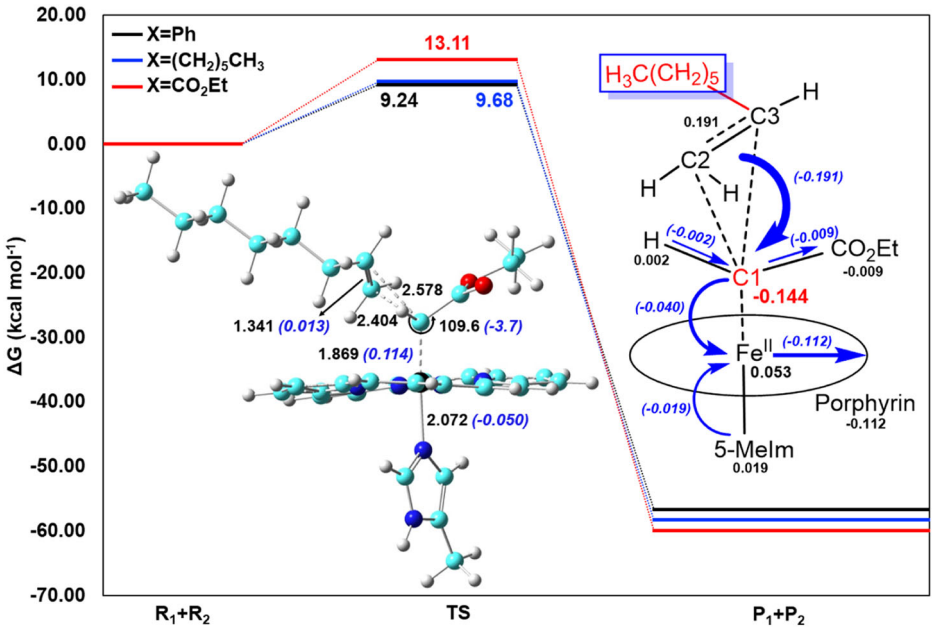

Fig. 3 | Free energy diagram of cyclopropanation pathways of different olefins in reactions 1–3. Key geometric parameters at transition state (in black), changes from reactants to transition state (in blue), atomic charge changes to transition state (in black), and charge transfers (in blue) as indicated by arrows and numbers in parentheses for reaction 2 (X = $(CH_2)_5CH_3$). Reaction barriers are shown around the TS energy levels. Atom color scheme: Fe, black; O, red; C, cyan; H, gray; N, blue.

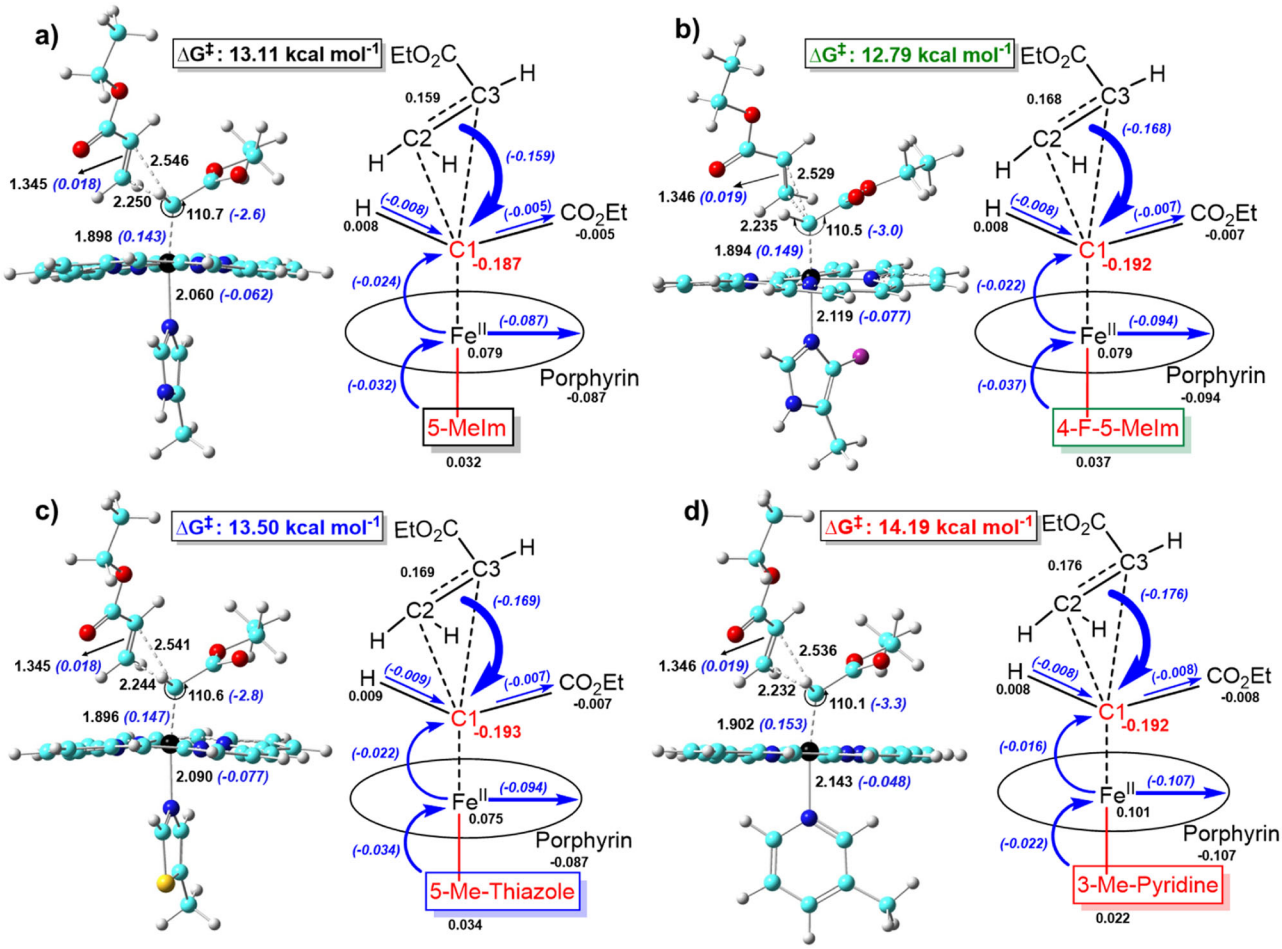

Fig. 4 | Key geometric parameters at transition state (in black) and changes from reactants to transition state (in blue), and atomic charge changes from reactants to transition state (in black) and charge transfers (in blue). a Reaction **3**; **b** Reaction **4**; **c** Reaction **5**; **d** Reaction **6**. Atom color scheme: Fe, black; O, red; C, cyan; H, gray; N, blue; F, purple; S, yellow.

Overall, these results provide the first computational assessment of non-native axial ligand effects on heme carbene cyclopropanations. This study shows that the previously used best native His ligand remains an optimal choice for cyclopropanation catalysis, whereas the 4-F-5-MeIm ligand is slightly better (~2-fold).

Effect of experimentally used macrocycles

Seeing that it is difficult to achieve significant reactivity improvement for the most challenging substrate, ethyl acrylate, by employing non-native axial ligands, we then studied the equatorial ligands. In this section, we examine the three experimentally employed macrocycles in cyclopropanations of styrene with the same His ligand within the myoglobin framework[9,14,15], which are modeled in reactions **7**–**9** for heme b, chlorin e6, and substituted porphycene, respectively. To better simulate the protein experimental results, His was truncated at the Cα position to become 5-ethylimidazole (5-EtIm), and the macrocycles' substituents were maintained, except that the terminal propionic groups (see Fig. 1) were substituted for propyl groups to avoid artificial H-bonding interactions in such truncated models, as done before[33,34,72].

Comparing the previously studied reaction involving porphyrin[54] (lacking the ring substitutions present on heme b) with an energy barrier of 9.24 kcal mol^{-1} and the analogous reaction **7** for heme b, the favorable effect of the ring substitutions is clear, as the latter possesses a barrier by 0.83 kcal mol^{-1} lower.

The use of chlorin e6 in reaction **8** results in an even lower $\Delta G^{\ddagger}$ of 5.75 kcal mol^{-1} than that for heme b in reaction **7**, 8.41 kcal mol^{-1}. This computational trend is in good agreement with the experimental observation that chlorin e6-substituted myoglobin variant Mb(H64V, V68A) performed significantly better than the same protein environment with the native heme b cofactor: >990 TTN vs. 434 TTN, respectively[15].

Prior experimental work also showed that after the wild type myoglobin (with heme b) was reconstituted with the substituted porphycene (see Fig. 1), a 35 times higher turnover frequency for the cyclopropanation of styrene was found[14]. As seen from Table 1 and Fig. 5, our computational work supports that this macrocycle is able to significantly bring down the energy barrier by 3.10 kcal mol^{-1} than the heme b counterpart.

These computational findings clearly support the experimental endeavors in using substituted macrocycles and variations of heme-like cofactors to improve catalytic cyclopropanation reactivity[73].

As shown in Fig. 6 and Supplementary Fig. 1 for key geometry and charge variations from reactants to transition states for these experimentally used macrocycles, respectively, the most significant geometric parameter change, atomic charge change, and charge transfer of these experimentally studied systems in reactions **7**–**9** remain the same as found in reactions **1**–**6**, discussed in previous sections. However, the larger and more complex macrocycle structures in reactions **7**–**9**, compared to the unsubstituted porphyrin in reactions **1**–**6**, induce more complicated interactions between macrocycle and carbene/substrate, making it difficult to correlate the reaction barrier with a single significant parameter. For instance, the ethyl group of the ester moiety in carbene with the porphycene system is closer to the macrocyclic side chains than the other two cases, which modifies the orientation of the CO_2Et group and introduces additional molecular

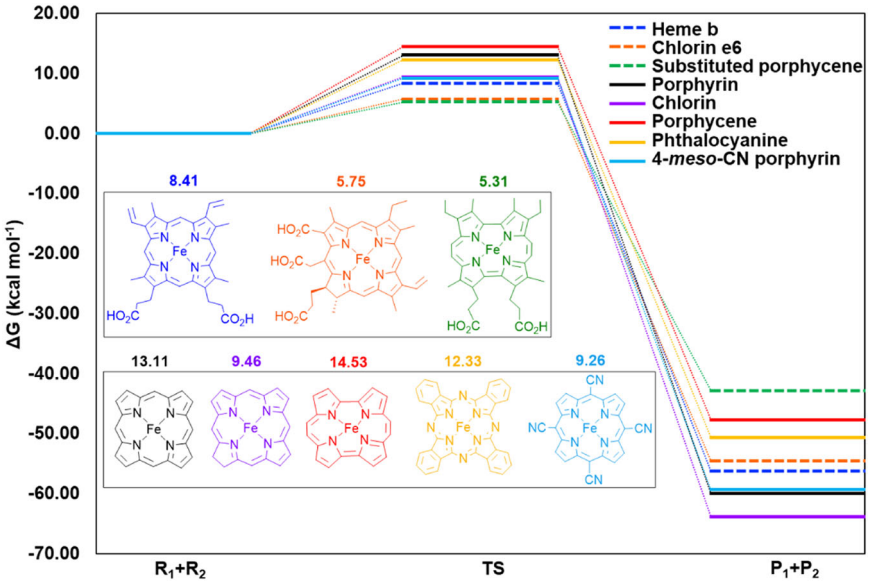

Fig. 5 | Free energy diagram of the cyclopropanation pathways of all eight macrocycles investigated in this study. Dashed lines throughout represent reactions of olefin **1** (X=Ph), and solid lines throughout represent reactions of olefin **3** (X = CO_2Et) with respective structures and energy barriers.

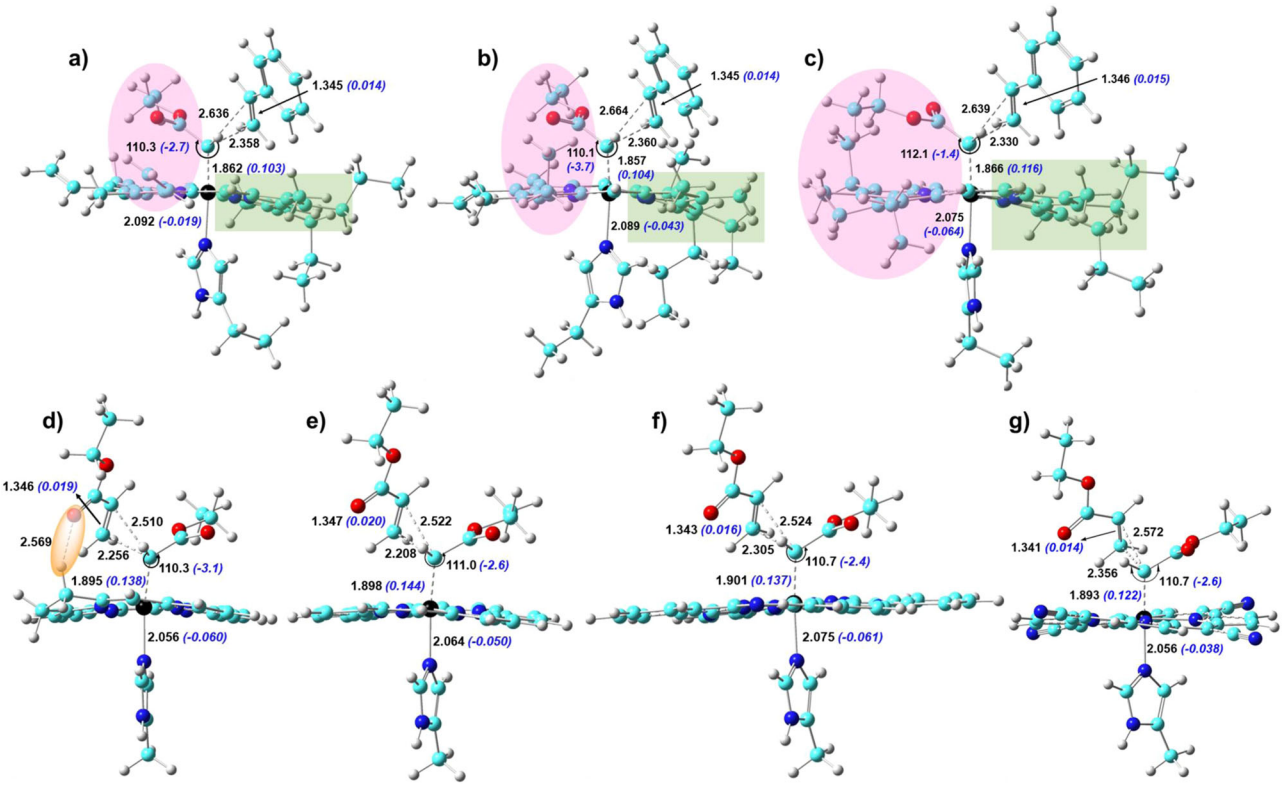

Fig. 6 | Key geometric parameters at transition state (in black) and changes from reactants to transition state (in blue). a Reaction **7**; **b** Reaction **8**; **c** Reaction **9**; **d** Reaction **10**; **e** Reaction **11**; **f** Reaction **12**; **g** Reaction **13**. Atom color scheme: Fe, black; O, red; C, cyan; H, gray; N, blue.

interactions (see pink color boxed areas in Fig. 6a–c). Another evident difference between the **TS** structures of the experimentally used macrocycles and those with the simple porphyrin is that the macrocycle planes in reactions **7–9** are severely distorted due to the extra 8-9 substituents (see the light green color boxed areas in Fig. 6a–c vs. those in Figs. 3 and 4).

The above work provides the first computational results to show favorable cyclopropanation energy barriers due to the employment of these experimentally used substituted macrocycles, particularly the value of non-heme macrocycles, which helps point to an important direction of new catalytic development.

Effect of macrocycles not being experimentally used yet

Given the favorable catalytic performance of various macrocycles and the complexity involved in the detailed geometric and electronic analysis of the above heavily substituted systems, we then investigated the pure effects of several commonly known porphyrin-like unsubstituted macrocycles in reactions **10–12** (as shown in Fig. 1) and compare with porphyrin to determine which non-natural macrocycle is most effective in minimizing the energy barrier. Importantly, all macrocycles investigated in this section have not been studied in experimental settings yet and this is the first computational study to report on their catalytic activities for this type of reaction.

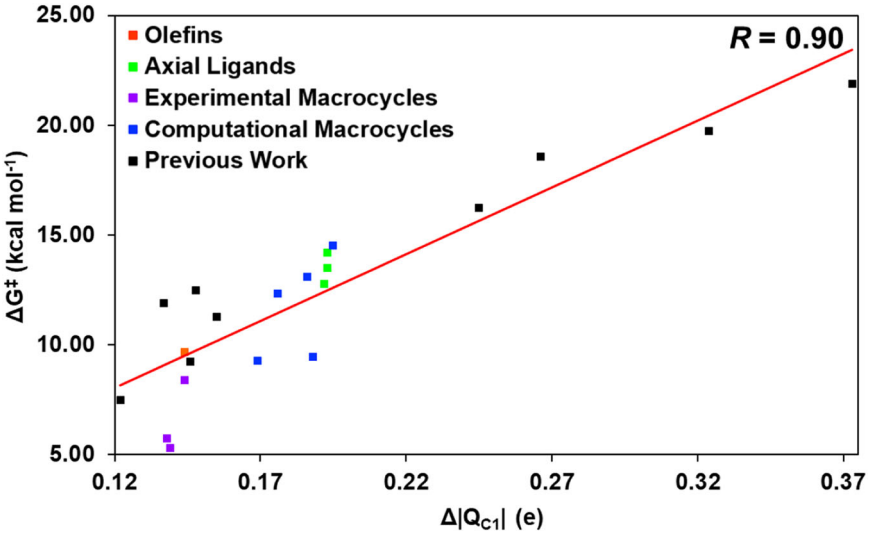

Fig. 7 | Plot of $\Delta G^{\ddagger}$ vs $\Delta|Q_{C1}|$ of data from this study and previous work[54] (shown as black blocks). Datapoints are colored based on their respective features and reaction numbers in the text.

Another goal is to determine whether any of these basic, non-native rings without substitutions can significantly reduce the reaction barrier for the cyclopropanation of the most challenging, electron-deficient substrate, ethyl acrylate, to a level comparable to the cyclopropanation of styrene with simple porphyrin, for which the substituted version (heme b) has been successfully realized experimentally in engineered heme biocatalysts[9]. If so, we expect adding substituents to such simple macrocycles, similar to prior experimental work, could enable this challenging cyclopropanation reaction to occur with similarly engineered heme proteins. As such, the unsubstituted chlorin and porphycene were studied and compared to porphyrin. Furthermore, the macrocycle phthalocyanine has been found to be active in styrene cyclopropanation in various experimental studies, as well as a recent computational study that reported good tolerance of dimeric complexes with electron-withdrawing olefins; however, mechanistic details of monomeric phthalocyanine complexes are limited[66,74–77], and its effect on cyclopropanation of ethyl acrylate has not been reported. So, the unsubstituted phthalocyanine was also investigated.

As shown in Fig. 5, these four macrocycles without substitutions alone cause a significant barrier range of 5.07 kcal mol^{-1}, indicating the potential modulation of reactivity even at the basic macrocycle level. Compared to porphyrin, which has $\Delta G^{\ddagger}$ of 13.11 kcal mol^{-1}, chlorin has the highest reactivity improvement and minimizes the barrier to 9.46 kcal mol^{-1}, which is close to $\Delta G^{\ddagger}$ of 9.24 kcal mol^{-1} for the cyclopropanation of styrene by porphyrin (reaction **1**, the reference point and barrier goal for the most challenging substrate, ethyl acrylate). The use of phthalocyanine also lowers the barrier, but the improvement of 0.78 kcal mol^{-1} is modest. In contrast, porphycene has an elevated $\Delta G^{\ddagger}$ of 14.53 kcal mol^{-1}, which is 1.42 kcal mol^{-1} higher than porphyrin. Interestingly, the reactivity trend for unsubstituted porphycene vs. porphyrin is different from that for the substituted counterparts studied in the former section, which highlights the critical role of substitution in improving reactivity. As such, we then studied a non-natural substitution containing four electron-withdrawing cyano groups at the meso position of the reference macrocycle porphyrin, i.e. 4-*meso*-CN porphyrin, which is designed to enhance the electronic driving force to facilitate the charge transfer from olefin to IPC, as found in these reactions (see Figs. 3 and 4). As seen from Fig. 5, $\Delta G^{\ddagger}$ of this reaction (**13**) shows that 4-*meso*-CN porphyrin is the most effective in lowering the energy barrier for all studied reactions for ethyl acrylate here.

Regarding key structural changes due to reactions going from reactants to transition states for these computationally studied non-native macrocycles (**10–13**), they still possess early **TS** features as **TS** geometries are more like reactants than products. For instance, C=C bond lengths in **TS** compared to $\mathbf{R_2}$ (ΔR_{C2C3}) are within 0.020 Å (Table 1), which are ~8-fold smaller than those compared to $\mathbf{P_2}$, ~0.160 Å (Supplementary Table 16). The most significant change is still the elongation of iron-carbene distance (R_{FeC1}), see Fig. 6. In general, as shown in Table 1, ΔR_{C2C3} increases with $\Delta G^{\ddagger}$ except for reaction **10**, which has the lowest barrier among four different basic macrocycles (**3, 10–12**). It is interesting to note that **TS**(**10**) experiences a significant distortion in one peripheral area of chlorin due to the presence of two sp^3 carbons, leading to one of the H on the macrocycle near the carbonyl O on the substrate to form a weak O–H interaction (distance of 2.569 Å), see the orange color box in Fig. 6d. It is known that the hydrogen bonding interaction can help reduce reaction barrier without significant effect on charge change[54,69], providing an additional means to reduce reaction barrier.

As seen from Supplementary Fig. 2, the most significant atomic charge change at **TS** from reactants is still associated with the carbene's carbon, and the largest charge transfer is also from the olefin to the carbene, i.e., the major charge features are the same in all the reactions **1–13**. In fact, a strong correlation between $\Delta|Q_{C1}|$, the absolute change in charge of the carbene carbon (which becomes more negatively charged as a result of the electrophilic attack, as discussed earlier), and the Gibbs free energy barrier, was found upon examination of various parameters exhibited by the 12 new IPC derivatives investigated in this work and previously reported 9 heme carbene cyclopropanations calculated using the same method ($R = 0.90$; Fig. 7)[54]. This result indicates the important role of carbene's electrophilicity in these reactions, which exhibits the effect of lower charge changes with lower energy barriers, corresponding to the more favorable early transition state features. Of course, other features may also be employed to modulate carbene's reactivity, as discussed in the section on experimentally used macrocycles. In fact, as seen from Fig. 7, datapoints for these three experimentally used macrocycles (purple datapoints) are more off the correlation line due to additional interactions from their more complex structures, and the correlation coefficient R can be improved to 0.93 if these datapoints are removed.

Conclusions

This work is of interest for a number of reasons. First, it provides the first direct computational comparisons of the reactivity differences among three characteristic substrates: the electron-rich styrene, the unactivated 1-octene, and the electron-deficient ethyl acrylate. Results reproduced the expected trend but offered previously unknown structural and electronic insights to understand the overall early **TS** feature and the key geometric and charge changes, particularly the electronic origin of the significantly challenging reactivity nature of ethyl acrylate. Second, it is the first computational assessment of various kinds of non-native axial ligands (substitution, heteroatom, ring size) on heme carbene cyclopropanations for the most challenging substrate (ethyl acrylate). Calculations show that the previously used native His ligand remains the optimal choice, while the addition of an

electron-withdrawing substituent to enhance the electronic driving force slightly increases reactivity. Third, the experimentally studied cofactors (heme b, chlorin e6, and substituted porphycene) in the heme protein framework in cyclopropanations of styrene were calculated for the first time. Results again reproduced the experimental reactivity trends and supported the favorable use of non-heme macrocycles for catalytic development. More importantly, a detailed analysis revealed the structural effects of the heavily substituted macrocycles, which induce more interactions with the carbene moiety and distort the macrocycle planarity. Fourth, this work discloses the first mechanistic information of non-native macrocycles (both unsubstituted porphyrin analogs and a substituted porphyrin) regarding their potential to catalyze the cyclopropanation of the challenging ethyl acrylate. It is interesting to see a significant barrier range of >5 kcal mol^{-1} for several different macrocycles with and without substitutions. Results also show that substitution can modulate and even reverse the reactivity trend. Both the basic chlorin and 4-*meso*-CN porphyrin macrocycle were found to be the most effective in reducing the cyclopropanation barriers for ethyl acrylate to the level for styrene, as used in prior successful experimental heme-based or inspired biocatalytic work. These results highlight the value of using heme-like macrocycles in biocatalytic cyclopropanation and suggest that it is possible to tame the very challenging ethyl acrylate with carefully designed Fe-based macrocycles in the heme protein framework. Fifth, the good agreements between theory and experiment here and the capability to identify some complicated interactions and mechanistic details also support the potential use of the computational tools to prescreen new macrocycle designs to save time and cost in heme-inspired biocatalyst development. Future studies to include the protein environment effect with experimental validations are needed to offer more complete assessment of these ideas in biocatalytic reactions of challenging electron-deficient olefins. Overall, this study provides many useful and novel mechanistic insights to help design efficient biocatalysts for the sustainable synthesis of cyclopropanes with challenging substrates.

Methods

All calculations were performed using the Gaussian 09 program[78]. All models investigated in this work were subject to full geometry optimizations without any symmetry constraints using the PCM method[79]. As our focus in this work is to compare different reactions from changes in the reaction center (cofactor, ligand, substrate) on the same footing, we chose the typical dielectric constant value of 4.0 used in some prior work of similar heme proteins and other proteins[33,34,47,54,70,80–86]. Compared to this value of 4.0, additional calculations using a high-end dielectric constant value of 78.3553 for the pure aqueous solvent environment (~20-fold increase) only increased the reaction barrier by 1.22 kcal mol^{-1} for the heme carbene formation reaction. As a protein contains many non-polar residues and is much less polar than water, the impact on the absolute value of the reaction barrier will be much less than this value. In fact, the current use of the dielectric constant of 4.0 enabled accurate quantitative predictions of experimental heme reaction barriers (e.g. an average error of 0.11 kcal mol^{-1} [84]) and experimental non-heme reaction barriers (e.g. an error of 0.36 kcal mol^{-1} [85]) besides reproducing reactivity trends of a number of biocatalytic heme carbene and nitrene transfer reactions[33,34,47,54,70,86].

After geometry optimization was done as described above, the frequency analysis was used to verify the nature of the stationary points on respective potential energy surfaces and to provide zero-point energy corrected electronic energies (E_{ZPE}'s), enthalpies (H's), and Gibbs free energies (G's) at 1 atm and room temperature, as used in experimental work for engineered heme biocatalysts[6–14,16–18,21,22,37–47]. In addition to the analysis of the vibrational modes of the imaginary frequencies (see Supplementary Table 18), intrinsic reaction coordinate calculations, as implemented in Gaussian 09, were also used to verify that the calculated cyclopropanation transition states correspond to the studied reactants and cyclopropanation products. The atomic charges and spin densities reported here are from the natural population analysis (NPA) and Mulliken schemes, respectively, as implemented in Gaussian 09. The NPA charge results were found to be consistent with experimentally found electrophilicity and reaction trends of several different kinds of heme carbene reactions[47,54,68–70]. Relative Gibbs free energies and select geometry, charge, and spin density results were discussed here, while all absolute values of electronic energies, zero-point energy corrected electronic energies, enthalpies, Gibbs free energies, all relative energies, key geometric parameters, charges, spin states, and other details are in the Supplementary Tables 1–17. 3D structures and Cartesian coordinates of optimized structures of the most favorable conformations are available in Supplementary Data File 1.

Recent studies on iron porphyrin carbenes and their reactions have investigated different DFT functionals and basis sets[54,67–69]. These methodological studies show that accurate predictions of various experimental properties of heme carbenes can be modeled by the range-separated hybrid DFT method with dispersion correction, ωB97XD[33,34,47,54,67–70]. The basis set includes the effective core potential (ECP) basis LanL2DZ[87] for iron and the triple-ζ basis 6-311 G* for all other elements, based on its accurate predictions from reactions involving heme carbene systems[33,34,47,54,67–70]. The use of a much larger 6-311 + + G(2 d,2p) basis for all non-metal atoms was found to yield similar results for heme carbene reactions[68] and thus further support the efficient use of the current basis set here. The use of an ECP basis for metal here is common in many reaction studies involving transition metal carbenoids, such as Ir porphyrin carbene[88], Ru porphyrin carbene[89], Rh carbene[90]. The advantage of an ECP basis is the inclusion of a relativistic effect basically absent in an all-electron basis set. In addition, it is available for all transition metals, which may allow direct comparisons of the effects of a vast amount of metal centers. The alternative use of an all-electron basis for the metal center[54] was recently found to yield qualitatively the same conclusions of geometric, electronic, and energetic features for heme carbene reactions, and therefore supports the use of LanL2DZ basis here, which may help direct comparisons with late transition metals in future studies, for which ECP basis is more readily available and commonly used. As there are no experimental energy barrier results in this area to provide benchmark data for computational predictions of absolute values of reaction barriers, we focus on relative barrier trends here. In fact, this method has enabled both qualitative reactivity trends for (1) experimental IPC formation[69], (2) C-H insertion[68], (3) cyclopropanation[54], (4) Si-H insertion[70], (5) chemoselectivity of cyclopropanation vs. C-H insertion[34], (6) diastereoselectivity of cyclopropanation[54], and quantitative predictions of (1) kinetic isotope effect for C-H insertion[68], cyclopropanation[54], and Si-H insertion[70], (2) ee and (3) de data of cyclopropanations[33] for a wide range of substrates. In addition, it exhibited excellent performance in quantitative predictions of experimental X-ray geometries with 1.0% mean percentage deviation[67], and yielded an excellent correlation between computed ^{13}C NMR chemical shieldings and experimental ^{13}C NMR chemical shifts ($R^2 = 0.9691$)[67]. To further evaluate the reactivity trends of the studied reactions, additional calculations using a large 6-311 + + G(2 d,2p) for all atoms were performed on each optimized structure to obtain the single point correction as a difference of electronic energies between this higher-level basis set and the above-mentioned basis set. This correction was then added to the free energy of each optimized species to generate its corrected free energy, which was subsequently used to calculate the high-level free energy barrier reported in Table 1.

The favorable spin states for the studied species were also selected based on the recent detailed spin state studies of the same or similar systems[47,54,69,70], i.e. singlet spin states for both reactants, transition states, and $\mathbf{P_2}$, and the quintet spin state for $\mathbf{P_1}$. For more information on detailed spin state studies, see Supplementary Note 1 and Supplementary Table 1.

As this work is focused on investigating the effects of various structural components on reactivities, not enantioselectivities, the chiralities of the calculated molecules were taken from similar previous reports[33,54] so as to compare with prior results on the same footing: for reactions **1**–**6** and **10**–**13**, the chirality is Pro RR for **TS** and RR for $\mathbf{P_2}$, and for reactions **7**–**9**, the chirality is Pro SS for **TS** and SS for $\mathbf{P_2}$.

Data availability

Data that supports the findings of this study are included in this published article and its supplementary information. 3D structures and Cartesian coordinates of optimized structures of the most favorable conformations are available in Supplementary Data File 1.

Received: 24 April 2024; Accepted: 19 November 2024;
Published online: 29 November 2024

References

1. Talele, T. T. The "Cyclopropyl Fragment" is a versatile player that frequently appears in preclinical/clinical drug molecules. *J. Med. Chem.* **59**, 8712–8756 (2016).
2. Wessjohann, L. A., Brandt, W. & Thiemann, T. Biosynthesis and metabolism of cyclopropane rings in natural compounds. *Chem. Rev.* **103**, 1625–1648 (2003).
3. Godula, K., Bärmann, H. & Donaldson, W. A. A simple and efficient synthesis of optically pure tricarbonyl(methyl 6-oxo-2,4-hexadienoate)iron. *J. Org. Chem.* **66**, 3590–3592 (2001).
4. Reichelt, A. & Martin, S. F. Synthesis and properties of cyclopropane-derived peptidomimetics. *Acc. Chem. Res.* **39**, 433–442 (2006).
5. Gnad, F. & Reiser, O. Synthesis and applications of β-aminocarboxylic acids containing a cyclopropane ring. *Chem. Rev.* **103**, 1603–1624 (2003).
6. Coehlo, P. S., Brustad, E. M., Kannan, A. & Arnold, F. H. Olefin cyclopropanation via carbene transfer catalyzed by engineered cytochrome P450 enzymes. *Science* **339**, 307–310 (2013).
7. Coehlo, P. S. et al. A serine-substituted P450 catalyzes highly efficient carbene transfer to olefins in vivo. *Nat. Chem. Biol.* **9**, 485–487 (2013).
8. Wang, Z. J. et al. Improved cyclopropanation activity of histidine-ligated cytochrome P450 enables the enantioselective formal synthesis of levomilnacipran. *Angew. Chem. Int. Ed.* **53**, 6810–6813 (2014).
9. Bordeaux, M., Tyagi, V. & Fasan, R. Highly diastereoselective and enantioselective olefin cyclopropanation using engineered myoglobin-based catalysts. *Angew. Chem. Int. Ed.* **54**, 1744–1748 (2015).
10. Gober, J. G. et al. Mutating a highly conserved residue in diverse cytochrome P450s facilitates diastereoselective olefin cyclopropanation. *ChemBioChem* **17**, 394–397 (2016).
11. Bajaj, P., Sreenilayam, G., Tyagi, V. & Fasan, R. Gram-scale synthesis of chiral cyclopropane-containing drugs and drug precursors with engineered myoglobin catalysts featuring complementary stereoselectivity. *Angew. Chem. Int. Ed.* **55**, 16110–16114 (2016).
12. Tinoco, A., Steck, V., Tyagi, V. & Fasan, R. Highly diastereo- and enantioselective synthesis of trifluoromethyl-substituted cyclopropanes via myoglobin-catalyzed transfer of trifluoromethylcarbene. *J. Am. Chem. Soc.* **139**, 5293–5296 (2017).
13. Sreenilayam, G., Moore, E. J., Steck, V. & Fasan, R. Metal substitution modulates the reactivity and extends the reaction scope of myoglobin carbene transfer catalysts. *Adv. Synth. Cat.* **359**, 2076–2089 (2017).
14. Oohora, K. et al. Catalytic cyclopropanation by myoglobin reconstituted with iron porphycene: acceleration of catalysis due to rapid formation of the carbene species. *J. Am. Chem. Soc.* **139**, 17265–17268 (2017).
15. Sreenilayam, G., Moore, E. J., Steck, V. & Fasan, R. Stereoselective olefin cyclopropanation under aerobic conditions with an artificial enzyme incorporating an iron-chlorin e6 cofactor. *ACS Catal.* **7**, 7629–7633 (2017).
16. Gober, J. G. et al. P450-mediated non-natural cyclopropanation of dehydroalanine-containing thiopeptides. *ACS Chem. Biol.* **12**, 1726–1731 (2017).
17. Knight, A. M. et al. Diverse engineered heme proteins enable stereodivergent cyclopropanation of unactivated alkenes. *ACS Cent. Sci.* **4**, 372–377 (2018).
18. Brandenberg, O. F. et al. Stereoselective enzymatic synthesis of heteroatom-substituted cyclopropanes. *ACS Catal.* **8**, 2629–2634 (2018).
19. Villarino, L. et al. An artificial heme enzyme for cyclopropanation reactions. *Angew. Chem. Int. Ed.* **57**, 7785–7789 (2018).
20. Hayashi, T. et al. Capture and characterization of a reactive haem–carbenoid complex in an artificial metalloenzyme. *Nat. Catal.* **1**, 578–584 (2018).
21. Moore, E. J., Steck, V., Bajaj, P. & Fasan, R. Chemoselective cyclopropanation over carbene y-h insertion catalyzed by an engineered carbene transferase. *J. Org. Chem.* **83**, 7480–7490 (2018).
22. Chen, K., Zhang, S. Q., Brandenberg, O. F., Hong, X. & Arnold, F. H. Alternate heme ligation steers activity and selectivity in engineered cytochrome P450-catalyzed carbene-transfer reactions. *J. Am. Chem. Soc.* **140**, 16402–16407 (2018).
23. Wolf, J. R., Hamaker, C. G., Djukic, J. P., Kodadek, T. & Woo, L. K. Shape and stereoselective cyclopropanation of alkenes catalyzed by iron porphyrins. *J. Am. Chem. Soc.* **117**, 9194–9199 (1995).
24. Gross, Z., Galili, N. & Simkhovich, L. Metailoporphyrin catalyzed asymmetric cyclopropanation of olefins. *Tetrahedron Lett.* **40**, 1571–1574 (1999).
25. Hamaker, C. G., Mirafzal, G. A. & Woo, L. K. Catalytic cyclopropanation with iron(II) complexes. *Organometallics* **20**, 5171–5176 (2001).
26. Li, Y., Huang, J. S., Zhou, Z. Y., Che, C. M. & You, X. Z. Remarkably stable iron porphyrins bearing nonheteroatom-stabilized carbene or (Alkoxycarbonyl) carbenes: Isolation, X-ray crystal structures, and carbon atom transfer reactions with hydrocarbons. *J. Am. Chem. Soc.* **124**, 13185–13193 (2002).
27. Lai, T. S. et al. Alkene cyclopropanation catalyzed by Halterman iron porphyrin: participation of organic bases as axial ligands. *Dalton Trans.* **28**, 4845–4851 (2006).
28. Nicolas, I., Maux, P. L. & Simonneaux, G. Synthesis of chiral water-soluble metalloporphyrins (Fe, Ru,): new catalysts for asymmetric carbene transfer in water. *Tetrahedron Lett.* **49**, 5793–5795 (2008).
29. Le Maux, P., Nicolas, I., Chevance, S. & Simonneaux, G. Chemical reactivity of 6-diazo-5-oxo-l-norleucine (DON) catalyzed by metalloporphyrins (Fe,Ru). *Tetrahedron* **66**, 4462–4468 (2010).
30. Morandi, B. & Carreira, E. M. Iron-catalyzed cyclopropanation in 6M KOH with iN Situ Generation of Diazomethane. *Science* **335**, 1471–1474 (2012).
31. Morandi, B., Dolva, A. & Carreira, E. M. Iron-catalyzed cyclopropanation with glycine ethyl ester hydrochloride in water. *Org. Lett.* **14**, 2162–2163 (2012).
32. Carminati, D. M. et al. Designing 'Totem' C2-symmetrical iron porphyrin catalysts for stereoselective cyclopropanations. *Chem. Eur. J.* **22**, 13599–13612 (2016).
33. Tinoco, A. et al. Origin of high stereocontrol in olefin cyclopropanation catalyzed by an engineered carbene transferase. *ACS Catal.* **9**, 1514–1524 (2019).
34. Vargas, D. A., Khade, R. L., Zhang, Y. & Fasan, R. Biocatalytic strategy for highly diastereo- and enantioselective synthesis of 2,3-dihydrobenzofuran based tricyclic scaffolds. *Angew. Chem. Int. Ed.* **58**, 10148–10152 (2019).
35. Chandgude, A. L., Ren, X. & Fasan, R. Stereodivergent intramolecular cyclopropanation enabled by engineered carbene transferases. *J. Am. Chem. Soc.* **141**, 9145–9150 (2019).
36. Brandenberg, O. F., Chen, K. & Arnold, F. H. Directed evolution of a cytochrome p450 carbene transferase for selective functionalization of cyclic compounds. *J. Am. Chem. Soc.* **141**, 8989–8995 (2019).
37. Siriboe, M. G., Vargas, D. A. & Fasan, R. Dehaloperoxidase catalyzed stereoselective synthesis of cyclopropanol esters. *J. Org. Chem.* **88**, 7630–7640 (2023).

38. Schaus, L. et al. Protoglobin-catalyzed formation of cis-trifluoromethyl-substituted cyclopropanes by carbene transfer. *Angew. Chem. Int. Ed.* **62**, e202208936 (2023).
39. Mao, R. et al. Enantio- and diastereoenriched enzymatic synthesis of 1,2,3-polysubstituted cyclopropanes from (Z/E)-trisubstituted enol acetates. *J. Am. Chem. Soc.* **145**, 16176–16185 (2023).
40. Ren, X. et al. Highly stereoselective and enantiodivergent synthesis of cyclopropylphosphonates with engineered carbene transferases. *Chem. Sci.* **13**, 8550–8556 (2022).
41. Porter, N. J., Danelius, E., Gonen, T. & Arnold, F. H. Biocatalytic carbene transfer using diazirines. *J. Am. Chem. Soc.* **144**, 8892–8896 (2022).
42. Roelfes, G. Repurposed and artificial heme enzymes for cyclopropanation reactions. *J. Inorg. Biochem.* **222**, 111523 (2021).
43. Nam, D., Steck, V., Potenzino, R. J. & Fasan, R. A diverse library of chiral cyclopropane scaffolds via chemoenzymatic assembly and diversification of cyclopropyl ketones. *J. Am. Chem. Soc.* **143**, 2221–2231 (2021).
44. Carminati, D. M., Decaens, J., Couve-Bonnaire, S., Jubault, P. & Fasan, R. Biocatalytic strategy for the highly stereoselective synthesis of CHF(2)-containing trisubstituted cyclopropanes. *Angew. Chem. Int. Ed.* **60**, 7072–7076 (2021).
45. Ren, X., Liu, N., Chandgude, A. L. & Fasan, R. An enzymatic platform for the highly enantioselective and stereodivergent construction of cyclopropyl-delta-lactones. *Angew. Chem. Int. Ed.* **59**, 21634–21639 (2020).
46. Moore, E. J. & Fasan, R. Effect of proximal ligand substitutions on the carbene and nitrene transferase activity of myoglobin. *Tetrahedron* **75**, 2357–2363 (2019).
47. Nam, D. et al. Mechanistic manifold in a hemoprotein-catalyzed cyclopropanation reaction with diazoketone. *Nat. Commun.* **14**, 7985 (2023).
48. Sosa Alfaro, V. et al. YfeX—a new platform for carbene transferase development with high intrinsic reactivity. *Chem. Eur. J.* **28**, e202201474 (2022).
49. Chen, Y., Ruppel, J. V. & Zhang, X. P. Cobalt-catalyzed asymmetric cyclopropanation of electron-deficient olefins. *J. Am. Chem. Soc.* **129**, 12074–12075 (2007).
50. Key, H. M., Dydio, P., Clark, D. S. & Hartwig, J. F. Abiological catalysis by artificial haem proteins containing noble metals in place of iron. *Nature* **534**, 534–537 (2016).
51. Smith, D. A., Reynolds, D. N. & Woo, L. K. Cyclopropanation catalyzed by osmium porphyrin complexes. *J. Am. Chem. Soc.* **115**, 2511–2513 (1993).
52. Anding, B. J., Ellern, A. & Woo, L. K. Olefin cyclopropanation catalyzed by iridium(III) porphyrin complexes. *Organometallics* **31**, 3628–3635 (2012).
53. Cristina Silva Costa, D. Additions to non-activated alkenes: Recent advances. *Arab. J. Chem.* **13**, 799–834 (2020).
54. Wei, Y., Tinoco, A., Steck, V., Fasan, R. & Zhang, Y. Cyclopropanations via heme carbenes: basic mechanism and effects of carbene substituent, protein axial ligand, and porphyrin substitution. *J. Am. Chem. Soc.* **140**, 1649–1662 (2018).
55. de Brito Sa, E., Rimola, A., Rodriguez-Santiago, L., Sodupe, M. & Solans-Monfort, X. Reactivity of metal carbenes with olefins: theoretical insights on the carbene electronic structure and cyclopropanation reaction mechanism. *J. Phys. Chem. A* **122**, 1702–1712 (2018).
56. Su, H., Ma, G. & Liu, Y. Theoretical insights into the mechanism and stereoselectivity of olefin cyclopropanation catalyzed by two engineered cytochrome P450 enzymes. *Inorg. Chem.* **57**, 11738–11745 (2018).
57. Torrent-Sucarrat, M., Arrastia, I., Arrieta, A. & Cossío, F. P. Stereoselectivity, different oxidation states, and multiple spin states in the cyclopropanation of olefins catalyzed by Fe–porphyrin complexes. *ACS Catal.* **8**, 11140–11153 (2018).
58. Casali, E., Gallo, E. & Toma, L. An in-depth computational study of alkene cyclopropanation catalyzed by Fe(porphyrin)(OCH3) complexes. the environmental effects on the energy barriers. *Inorg. Chem.* **59**, 11329–11336 (2020).
59. Rogge, T., Zhou, Q., Porter, N. J., Arnold, F. H. & Houk, K. N. Iron heme enzyme-catalyzed cyclopropanations with diazirines as carbene precursors: computational explorations of diazirine activation and cyclopropanation mechanism. *J. Am. Chem. Soc.* **146**, 2959–2966 (2024).
60. Meunier, B., de Visser, S. P. & Shaik, S. Mechanism of oxidation reactions catalyzed by cytochrome P450 enzymes. *Chem. Rev.* **104**, 3947–3980 (2004).
61. Shaik, S., de Visser, S. P., Ogliaro, F., Schwarz, H. & Schröder, D. Two-state reactivity mechanisms of hydroxylation and epoxidation by cytochrome P-450 revealed by theory. *Curr. Opin. Chem. Biol.* **6**, 556–567 (2002).
62. Wang, Z. et al. How the conformational movement of the substrate drives the regioselective C–N bond formation in P450 TleB: insights from molecular dynamics simulations and quantum mechanical/molecular mechanical calculations. *J. Am. Chem. Soc.* **145**, 7252–7267 (2023).
63. Sharon, D. A., Mallick, D., Wang, B. & Shaik, S. Computation sheds insight into iron porphyrin carbenes' electronic structure, formation, and N−H insertion reactivity. *J. Am. Chem. Soc.* **138**, 9597–9610 (2016).
64. Chaturvedi, S. S. et al. Can second coordination sphere and long-range interactions modulate hydrogen atom transfer in a non-heme Fe(II)-dependent histone demethylase? *JACS Au* **2**, 2169–2186 (2022).
65. Thomas, M. G. et al. The unique role of the second coordination sphere to unlock and control catalysis in nonheme Fe(II)/2-oxoglutarate histone demethylase KDM2A. *Inorg. Chem.* **63**, 10737–10755 (2024).
66. Lemon, C. M. Diversifying the functions of heme proteins with non-porphyrin cofactors. *J. Inorg. Biochem.* **246**, 112282 (2023).
67. Khade, R. L. et al. Iron porphyrin carbenes as catalytic intermediates: structures, Mossbauer and NMR spectroscopic properties, and bonding. *Angew. Chem. Int. Ed.* **53**, 7574–7578 (2014).
68. Khade, R. L. & Zhang, Y. C-H insertions by iron porphyrin carbene: basic mechanism and origin of substrate selectivity. *Chem. Eur. J.* **23**, 17654–17658 (2017).
69. Khade, R. L. & Zhang, Y. Catalytic and biocatalytic iron porphyrin carbene formation: effects of binding mode, carbene substituent, porphyrin substituent, and protein axial ligand. *J. Am. Chem. Soc.* **137**, 7560–7563 (2015).
70. Khade, R. L., Chandgude, A. L., Fasan, R. & Zhang, Y. Mechanistic investigation of biocatalytic heme carbenoid Si-H insertions. *ChemCatChem* **11**, 3101–3108 (2019).
71. Roy, S. et al. Stereodivergent synthesis of pyridyl cyclopropanes via enzymatic activation of pyridotriazoles. *J. Am. Chem. Soc.* **146**, 19673–19679 (2024).
72. Yang, L., Ling, Y. & Zhang, Y. HNO binding in a heme protein: structures, spectroscopic properties, and stabilities. *J. Am. Chem. Soc.* **133**, 13814–13817 (2011).
73. Damiano, C., Sonzini, P. & Gallo, E. Iron catalysts with N-ligands for carbene transfer of diazo reagents. *Chem. Soc. Rev.* **49**, 4867–4905 (2020).
74. Sharma, V. B., Jain, S. L. & Sain, B. Metallophthalocyanines as potent catalysts for cyclopropanation of olefins with ethyldiazoacetate. *Catal. Lett.* **94**, 57–59 (2004).
75. Ventura, D. L. & Kubiak, R. W. Metallophthalocyanine-catalyzed cyclopropanation. *Tetrahedron Lett.* **55**, 2715–2717 (2014).

76. Liu, H.-H. et al. Cyclopropanation of alkenes catalyzed by metallophthalocyanines. *J. Mol. Catal.* **246**, 49–52 (2006).
77. Cailler, L. P. et al. Comparative study of the electronic structures of μ-Oxo, μ-nitrido, and μ-carbido diiron octapropylporphyrazine complexes and their catalytic activity in cyclopropanation of olefins. *Inorg. Chem.* **59**, 1104–1116 (2020).
78. Frisch, M. J. et al. *Gaussian 09, Revision D.01* (Gaussian, Inc., Wallingford CT, 2013).
79. Mennucci, B. & Tomasi, J. Continuum solvation models: a new approach to the problem of solute's charge distribution and cavity boundaries. *J. Chem. Phys.* **106**, 5151–5158 (1997).
80. Torres, R. A., Lovell, T., Noodleman, L. & Case, D. A. Density functional and reduction potential calculations of Fe4S4 clusters. *J. Am. Chem. Soc.* **125**, 1923–1936 (2003).
81. Ullmann, M. G., Noodleman, L. & Case, D. A. Density functional calculation of pKa values and redox potentials in the bovine Rieske iron-sulfur protein. *J. Biol. Inorg. Chem.* **7**, 632–639 (2002).
82. Takano, Y. & Nakamura, H. Density functional study of roles of porphyrin ring in electronic structures of heme. *Int. J. Quantum Chem.* **109**, 3583–3591 (2009).
83. Blomberg, M. R. A., Borowski, T., Himo, F., Liao, R.-Z. & Siegbahn, P. E. M. Quantum chemical studies of mechanisms for metalloenzymes. *Chem. Rev.* **114**, 3601–3658 (2014).
84. Shi, Y. & Zhang, Y. Mechanisms of HNO reactions with ferric heme proteins. *Angew. Chem. Int. Ed.* **57**, 16654–16658 (2018).
85. Shi, Y., Michael, M. A. & Zhang, Y. HNO to NO conversion mechanism with copper zinc superoxide dismutase, comparison with heme protein mediated conversions, and the origin of questionable reversibility. *Chem. Eur. J.* **27**, 5019–5027 (2021).
86. Wei, Y., Conklin, M. & Zhang, Y. Biocatalytic intramolecular C-H aminations via engineered heme proteins: full reaction pathways and axial ligand effects. *Chem. Eur. J.* **28**, e202202006 (2022).
87. Hay, P. J. & Wadt, W. R. Ab initio effective core potentials for molecular calculations. Potentials for the transition metal atoms Sc to Hg. *J. Chem. Phys.* **82**, 270–283 (1985).
88. Wang, J.-C. et al. Highly enantioselective intermolecular carbene insertion to C–H and Si–H bonds catalyzed by a chiral iridium(III) complex of a D4-symmetric Halterman porphyrin ligand. *Chem. Commun.* **48**, 4299–4301 (2012).
89. Chan, K.-H., Guan, X., Lo, V. K.-Y. & Che, C.-M. Elevated catalytic activity of ruthenium(II)–porphyrin-catalyzed carbene/nitrene transfer and insertion reactions with N-heterocyclic carbene ligands. *Angew. Chem. Int. Ed.* **53**, 2982–2987 (2014).
90. Nakamura, E., Yoshikai, N. & Yamanaka, M. Mechanism of C-H bond activation/C-C bond formation reaction between diazo compound and alkane catalyzed by dirhodium tetracarboxylate. *J. Am. Chem. Soc.* **124**, 7181–7192 (2002).

Acknowledgements

This work was supported by the U.S. National Science Foundation (NSF) grant CHE-2054897 to Y.Z. We also acknowledge the support from the Provost's Office Undergraduate Research Funds at Stevens Institute of Technology to V.M.

Author contributions

Y.Z. conceived the idea and designed the research. D.J., V.M., and R.K. conducted the computational studies. All authors participated in the data analyses and preparation of data tables and figures. V.M. and Y.Z. wrote the manuscript together with input from all authors.

Competing interests

The authors declare no competing interests.

Additional information

Supplementary information The online version contains supplementary material available at https://doi.org/10.1038/s42004-024-01371-4.

Correspondence and requests for materials should be addressed to Yong Zhang.

Peer review information *Communications Chemistry* thanks the anonymous reviewers for their contribution to the peer review of this work.